THE SOUTHERN CHINA MONSOON RAINFALL EXPERIMENT (SCMREX)

Yali Luo, Renhe Zhang, Qilin Wan, Bin Wang, Wai Kin Wong, Zhiqun Hu, Ben Jong-Dao Jou, Yanluan Lin, Richard H. Johnson, Chih-Pei Chang, Yuejian Zhu, Xubin Zhang, Hui Wang, Rudi Xia, Juhui Ma, Da-Lin Zhang, Mei Gao, Yijun Zhang, Xi Liu, Yangruixue Chen, Huijun Huang, Xinghua Bao, Zheng Ruan, Zhehu Cui, Zhiyong Meng, Jiaxiang Sun, Mengwen Wu, Hongyan Wang, Xindong Peng, Weimiao Qian, Kun Zhao, and Yanjiao Xiao

A unique program is developed for improving heavy rainfall forecasts over southern China during the presummer rainy season through field campaigns and research on physical mechanisms and convection-permitting modeling.

The presummer rainy season (April–June) in southern China (Ding 1994), occurring during the early stage of the East Asian summer monsoon, accounts for about a half of the annual precipitation amount with maximum seasonal rainfall accumulation exceeding 800 mm in several areas (Fig. 1). The presummer rainy season in southern China reaches its peak frequency of heavy rainfall events and the maximum daily rainfall amount around the time of the onset of South China Sea (SCS) monsoon in May (Ding 1994, see Table 3.2 therein). The presummer rainy season ends when the monsoonal rain belt moves northward to the Yangtze River valley in east–central China in mid-June, when

AFFILIATIONS: Luo, R. Zhang, Hu, Hu. Wang, Xia, Gao, Y. Zhang, Bao, Ruan, Cui, Wu, Ho. Wang, and Peng—State Key Laboratory of Severe Weather, Chinese Academy of Meteorological Sciences, Beijing, China; Wan, X. Zhang, and Huang—Institute of Tropical and Marine Meteorology/Guangdong Provincial Key Laboratory of Regional Numerical Weather Prediction, Guangzhou, China; B. Wang and Xiao—Institute of Heavy Rainfall, Wuhan, China; Wong—Hong Kong Observatory, Hong Kong, China; Jou—Department of Atmospheric Sciences, National Taiwan University, Taipei, Taiwan; Lin—Ministry of Education Key Laboratory for Earth System Modeling, Center for Earth System Science, and Joint Center for Global Change Studies, Tsinghua University, Beijing, China; Johnson—Colorado State University, Fort Collins, Colorado; Chang—Naval Postgraduate School, Monterey, California; Zhu—NOAA/NCEP, College Park, Maryland; Ma—Collaborative Innovation Center on Forecast and Evaluation of Meteorological Disasters, Nanjing University of Information Science and Technology, Nanjing, China; D.-L. Zhang—State Key Laboratory of Severe Weather, Chinese Academy of Meteorological Sciences, Beijing, China, and Department of Atmospheric and Oceanic Science, University of Maryland, College Park, College Park, Maryland; Liu—Collaborative Innovation Center on Forecast and Evaluation of Meteorological Disasters, Nanjing University of Information Science and Technology, Nanjing, and State Key Laboratory of Severe Weather, Chinese Academy of Meteorological Sciences, Beijing, China; Chen—State Key Laboratory of Severe Weather, Chinese Academy of Meteorological Sciences, and University of Chinese Academy of Sciences, Beijing, China; Meng—Department of Atmospheric and Oceanic Sciences, School of Physics, Peking University, Beijing, China; Sun—CAAC East China Regional Air Traffic Administration, Shanghai, China; Qian—Shijiazhuang Meteorological Bureau, Shijiazhuang, China; Zhao—Nanjing University, Nanjing, China

CORRESPONDING AUTHOR: Yali Luo, yali@camscma.cn

The abstract for this article can be found in this issue, following the table of contents.

DOI:10.1175/BAMS-D-15-00235.1

In final form 26 August 2016

the mei-yu season starts there. Most precipitation during the presummer rainy season is of a convective nature with mesoscale organizational characteristics (Luo et al. 2013; Xia et al. 2015). The precipitation, mostly taking place hundreds of kilometers ahead (to the south) of a cold or quasi-stationary front (i.e., in the warm sector), normally has a larger accumulated rainfall amount than that closely associated with a cold frontal zone (Huang 1986; Ding 1994).

During the presummer rainy season, southern China and its vicinity often experience the most frequent occurrences of extreme rainfall, leading to severe flooding and inundations. These storms endanger the safety of lives and cause marked property damage, often producing devastating economic losses. To improve the scientific understanding and practical forecast of the presummer rainy season rainfall over southern China, three research and field programs were conducted in China during 1977–81 (Huang 1986), 1998 (Zhou 2003), and 2008/09 (Zhang et al. 2011), respectively, and their scientific achievements have been summarized by Luo (2017). However, there are still many unknowns about the mechanisms governing the formation and evolution of heavy rainfall over southern China during the presummer rainy season, especially those related to mesoscale convective systems (MCSs) and their interactions with larger-scale atmospheric systems because of the complicated multiscale atmospheric processes involved, the complex underlying surface (land–sea contrast, topography, and urban landscape; Fig. 1b), and the lack of comprehensive high-resolution observations. The skills of quantitative precipitation forecast (QPF) for the extreme rainfall that occurs in the warm sector over southern China during the presummer rainy season remain rather low for the global and regional models used at the National Meteorological Center of China in Beijing and the Regional Meteorological Center of South China in Guangzhou.

To expedite the efforts in improving the QPF during the presummer rainy season in southern China, the China Meteorological Administration (CMA) initiated the nationally coordinated research project, namely, the Southern China Monsoon Rainfall Experiment (SCMREX) that was endorsed by the World Meteorological Organization (WMO) in 2012 as a research and development project (RDP) of the World Weather Research Programme

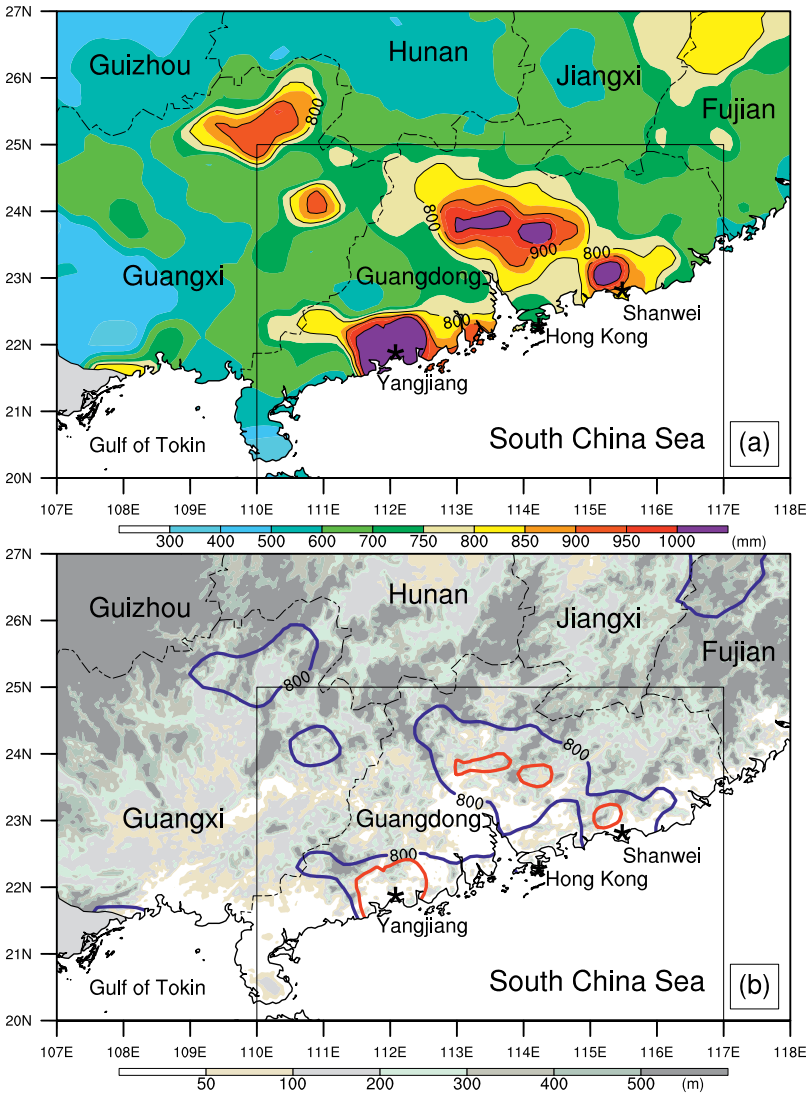

Fig. 1. (a) Distribution of the seasonal-mean rainfall accumulated during Apr–Jun of 1981–2012 based on the national surface meteorological stations over southern China. (b) Topography over southern China (shading), overlaid with 800- and 1,000-mm contours of the seasonal-mean rainfall that are denoted by blue and red lines, respectively. Thin dashed lines denote the borders between provinces. The names of the six provinces and the three coastal cities (stars) are labeled. Thin solid lines highlight the enhanced observing area (20°–25°N, 110°–117°E).

(WWRP). The scientific objectives of the SCMREX are 1) to better understand the physical mechanisms governing the initiation, evolution, morphology, organization, and duration of the heavy-rain-producing MCSs that determine the precise timing and location and accumulative amount of rainfall; 2) to better understand the microphysical and kinematic structures of the heavy-rain-producing MCSs that determine the instantaneous rainfall amount and are of relevance to validating parameterization schemes representing cloud–precipitation microphysical processes in numerical weather prediction (NWP) models; and 3) to improve finescale QPF skill by better understanding the multiscale precipitation processes, assessing the impact of assimilating high-resolution observations into convection-permitting (horizontal grid spacing of 1–4 km) numerical models of QPF, and evaluating and improving cloud microphysical parameterization schemes in convection-permitting models.

SCMREX RDP was originally planned to be a 3-yr project from 2013 to 2015 and later was extended to 2018 by WMO in October 2015. The RDP consists of four major components: a field campaign, database management, studies on physical mechanisms of heavy rainfall events, and convection-permitting NWP experiments including impact of data assimilation, evaluation/improvement of model physics, and ensemble prediction. The pilot field campaigns were carried out from early May to mid-June of 2013–15. A database system has been setup for sharing of observation data collected from the field campaigns. The data can be accessed through application online (http://scmrex.camscma.cn) where the implementation plan of SCMREX is also available.

FIELD CAMPAIGN. The field campaign component of SCMREX aims at obtaining composite high-density observations to detect the atmospheric environment and internal structures of the rainstorms during the presummer rainy season of southern China. The intensive observing periods (IOPs) of 2013 covered 15 days (8–17 and 24–28 May 2013), while the IOPs of 2014 and 2015 ran continuously from 1 May to 15 June. The observing regions covered Guangdong, southeastern Guangxi, Hainan, Hong Kong, and the offshore of SCS (Fig. 2a). The observing network was built upon the CMA's operational meteorological observing network consisting of the sounding stations, Doppler weather radars, wind-profiling radars (WPRs), automated weather stations (AWSs), Guangdong–Hong Kong–Macau lightning location system (LLS), and China's Fengyun (FY) satellites. The Doppler radars in southern China are similar to the Weather Surveillance Radar-1988 Doppler (WSR-88D) in the United States in both hardware and software (Zhu and Zhu 2004). A total of 17 boundary layer WPRs were deployed along the coastal areas of Guangdong and central Guangdong to continuously observe the mesoscale wind fields in the planetary boundary layer (PBL) and the lower troposphere that are of particular importance for studying convective initiation and development. Seventeen sensors were employed in the Guangdong–Hong Kong–Macau LLS (Fig. 2b) and the combined magnetic direction finding (MDF)/time of arrival (TOA) technology was used to detect cloud-to-ground lightning strike information (Cummins et al. 1998). The flash detection efficiency and stroke detection efficiency were about 95% and 90%, respectively, and the median value of location error was estimated to be about 410 m (Zhang et al. 2014). The *FY-2D* and *FY-2E* geostationary satellites generate 28 cloud images on a daily basis under normal operation schedule, whereas each of the *FY-3A* and *FY-3B* polar-orbiting satellites collects imager and sounding data over the target area twice a day. The structures of MCSs, related kinematic or convection characteristics, and cloud–precipitation microphysical parameters can be inferred not only from the Doppler radars and the LLS measurements, but also from a series of portable remote sensing instruments deployed over Guangdong's western coastal region and the Pearl River delta area (Fig. 2b). Table 1 lists the major instruments that participated in the field campaigns.

During the SCMREX IOPs in 2013, four sounding stations in Guangdong Province launched two extra soundings per day (i.e., at 0600 and 1800 UTC) in addition to the routine observations at 0000 and 1200 UTC. During the 2014 and 2015 IOPs, respectively, five and six sounding stations in Guangdong, Hainan, and Hong Kong launched two extra soundings per day, while three and two sounding stations in eastern and southeastern Guangxi launched one extra sounding per day (at 0600 UTC), with another extra sounding per day (at 1800 UTC) only for 10 days of each IOP. Moreover, a research flight was conducted by the Government Flying Service (GFS) of Hong Kong during the morning (around 2300–0200 UTC) on 16 June 2014 after its overhaul maintenance. It has been planned to collect observations over the Hong Kong Flight Information Region (green lines in Fig. 2a) using a new aircraft with both the dropsonde measurement system and in situ data probe during the extended period of experiments in 2017/18.

To obtain information about microphysical properties and kinematic structure of the rainstorms, the field campaigns deployed a number of portable instruments including two C-band polarimetric (C-POL) radars, one C-band frequency-modulated continuous wave (C-FMCW) radar, two 8-mm wavelength cloud radars (MMCR), one micro rain radar (MRR), several raindrop disdrometers, and one microwave radiometer (Fig. 2b; Table 1). These instruments mostly participated in the field experiments in both 2013 and 2014, although the locations of some instruments slightly changed between the 2 years. To facilitate the wind retrieval using dual-Doppler measurements, a C-POL radar was placed about 48.5 km to the southwest of the Guangzhou operational weather radar in the 2013 and 2014 IOPs (i.e., the Heshan C-POL radar in Fig. 2b), while another C-POL radar was placed 52.5 km northeast and 27.0 km northwest of the Yangjiang operational S-band radar in the 2013 and 2014 IOPs (labeled A2 and B2 in Fig. 2b). The MMCR and MRR were placed at Sanshui (labeled A1 in Fig. 2b) and Yangjiang (with the C-FMCW radar; labeled B1 in Fig. 2b) during the 2013 and 2014 IOPs, respectively. Specification of the MMCR, C-FMCW, and C-POL radars can be found in Liu et al. (2015, see Table 2 therein). Moreover, one S-band polarimetric (S-POL) radar started its normal operation at Zhuhai in early 2014, and its observational data during the 2014/15 IOPs were archived in the SCMREX database. The raindrop disdrometers were placed around the Yangjiang area in the 2013/14 IOPs and the Zhuhai area in the 2015 IOP to complement the polarimetric radars and facilitate estimation of raindrop size distribution. The other portable instruments (e.g., the C-POL radars, MMCR, and C-FMCW radar) did not participate in the 2015 IOP. More facilities will be used during the SCMREX 2016–18 field campaigns, including a two-dimensional video disdrometer (2DVD; Schönhuber et al. 2007) and one more C-POL radar.

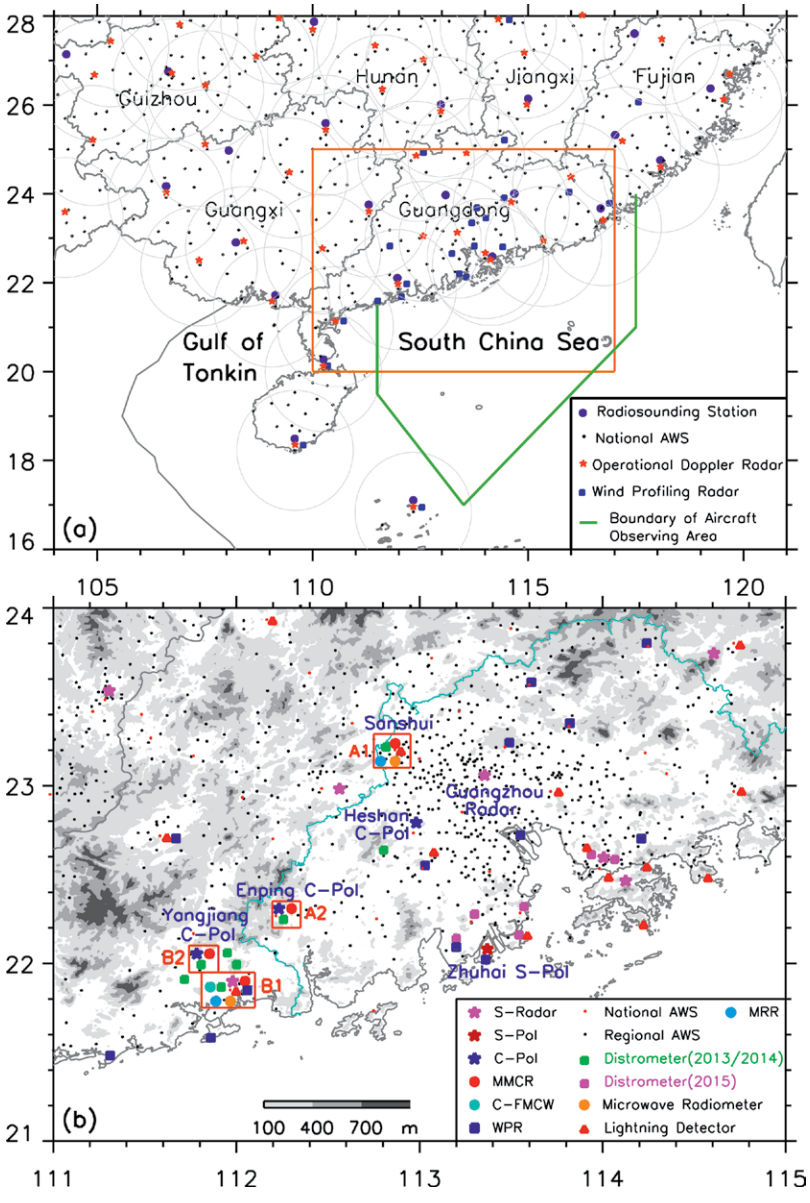

Fig. 2. Distribution of major observing facilities that participated during the SCMREX pilot field campaigns over (a) southern China and its vicinity and (b) central and western Guangdong Province where the portable instruments were placed during the 2013–15 IOPs. In (a), orange and green lines highlight the enhanced observing area (20°–25°N, 110°–117°E) and the aircraft observing area, respectively, and the circles with a radius of 150 km are centered at the operational S-band radars approximately representing their PPI scanning range. In (b), gray shading represents topography, the light blue line denotes the boundary of the Pearl River delta area, and A1 and A2 (B1 and B2) denote the locations with the most portable instruments during the 2013 (2014) IOPs. All the facilities are consistent with markers in the legend.

Table 1. Major instruments deployed during the SCMREX-2014 field campaign.		
Instrument or station	**Number**	**Coverage or location**
Automated weather station	1,946	21–25°N, 110°–117°E
Radiosonde station with additional launches	8 (3 in Guangdong, 1 in Hong Kong, 2 in southeastern Guangxi, and 2 in Hainan)	See Fig. 2a
Operational Doppler radar	14	21°–25°N, 110°–117°E
Polarimetric radar	3 (Zhuhai S-POL, Heshan C-POL, and Yangjiang C-POL radars)	22.027°N, 113.370°E; 22.737°N, 112.981°E; 22.011°N, 111.788°E
Wind-profiling radar	17	21°–25°N, 110°–117°E (see Fig. 2a)
Disdrometer	7	See Fig. 2b
MMCR	2	21.845°N, 111.979°E; 22.011°N, 111.788°E
Micro rain radar	1	21.845°N, 111.979°E
C-FMCW radar	1	21.845°N, 111.979°E
Microwave radiometer	1	21.845°N, 111.979°E
Lightning detector	17	14 are shown in Fig. 2b

OVERVIEW OF HEAVY RAINFALL EVENTS DURING THE SCMREX-2014 IOP. Figure 3 shows the time series of the number of rain gauges in Guangdong Province within the enhanced observing area (20°–25°N, 110°–117°E) that recorded extreme daily rainfall (>100 or >200 mm day^{-1}) and hourly rainfall (>20 mm h^{-1}) during the IOPs of 2013–15. It can be observed that a number of heavy rainfall events occurred during each IOP. For brevity of discussion, however, only the major heavy rainfall events during the 2014 IOP are described hereinafter. The most intense precipitation events during the 2014 IOP occurred on 8, 11, 22, and 23 May (Fig. 4) with daily rainfall of more than 100 mm recorded by 89, 155, 34, and 98 stations, respectively. On 11 and 23 May, the daily rainfall even exceeded 200 mm at 45 and 35 stations, respectively. Location of the most abundant rainfall varied notably among the days from the coastal regions as shown on 11 May (Fig. 4a) to the northern inland area such as 23 May (Fig. 4d).

Rainfall distribution and MCSs' evolution. On 8 May 2014, daily heavy rainfall exceeding 50 mm day^{-1} exhibits a west–east-oriented band extending from southeastern Guangxi to the Pearl River delta area in Guangdong, with the heaviest daily rainfall of 100–200 mm located in the east of the rainband (Fig. 4a). Numerous convective clusters were observed around southwestern Guangdong, southeastern Guangxi, and the adjacent ocean to the east of Zhanjiang (× in Figs. 5a and 5b) during late morning to early afternoon hours on 8 May (Fig. 5a). Although few convective clusters developed over the coastal waters, some developed over the land and grew in length, leading to the formation of a quasi-linear MCS over Guangdong coastal area in the late afternoon (Fig. 5b). This linear MCS lasted for 10 h, from 1600 Beijing standard time (BST; BST = UTC + 8 h; BST is earlier than the local solar time of Guangdong Province by approximately 11–41 min) 8 May to 0200 BST 9 May. The whole precipitation process contributed to about 90% of the daily rainfall amount over the Pearl River delta area and its west on 8 May 2014.

On 11 May, extreme rainfall affected the central coastal area of Guangdong, with more than 200 mm day^{-1} located mostly in the coastal region of the Pearl River delta region, while heavy precipitation of 100–200 mm day^{-1} fell over northern Guangxi (Fig. 4b). The extreme rainfall along the Guangdong coast on 11 May 2014 was generated mostly by two linearly shaped MCSs (labeled A1 and A2 in Figs. 5c and 5d) that sequentially moved along the coastline from Yangjiang to Shenzhen (× in Figs. 5c and 5d). The two MCSs had similar organizational characteristics, that is, consisting of northeastward "echo training" convective cells (Doswell et al. 1996). During their development, new convective cells were continuously initiated at the southwestern periphery of the MCSs, leading to the growth and sustained development of MCSs. Another linear MCS (labeled A3 in Figs. 5c and 5d) originated in Guangxi and then merged with the locally developed MCS A2 in the late afternoon (about 1700 BST).

On 22 May, widespread precipitation was distributed over Guangdong Province except for its southwestern portion (Fig. 4c). However, heavy rainfall of more than 100 mm day^{-1} was confined

over the northern mountains, showing a narrow and nearly west–east-oriented rainband, along which five rain gauges recorded more than 200 mm of daily precipitation (Fig. 4c). The extreme precipitation was produced sequentially by two MCSs (labeled B1 and B2 in Figs. 5e and 5f). The first MCS (B1) was initiated around midnight at the windward slope in northern Guangdong, and it was rather slow moving with a duration of about 9 h (0200–1300 BST). The other MCS (B2) was a squall line that was initiated over northern Guangxi in the late afternoon of the previous day, moved southeastward into Guangdong at about 1100 BST 22 May and passed across Guangdong in about 11 h. The quasi-stationary MCS B1 and the fast moving squall-line MCS B2, respectively, contributed about 60% and 40% of the total precipitation to this extreme rainfall event in northern Guangdong.

On 23 May, daily precipitation exceeding 50 mm day^{-1} showed a broad band extending from northern Guangdong southeastward to the coastal region from Hong Kong to Shanwei (circles in Fig. 4d), with the precipitation of more than 200 mm day^{-1} located mostly over central Guangdong and its coasts

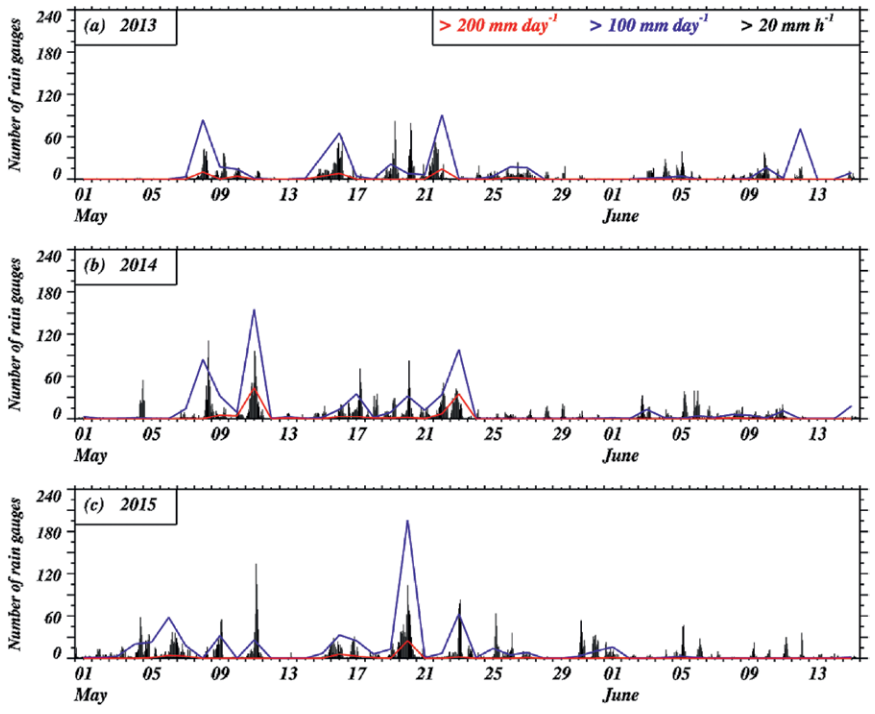

Fig. 3. Time series of the number of rain gauges in Guangdong Province within the SCMREX enhanced observing area (orange rectangle in Fig. 2b) that recorded extreme daily rainfall (>200 mm day^{-1}, red lines; >100 mm day^{-1}, blue lines) and heavy hourly rainfall (>20 mm h^{-1}, gray bars) during (a) 2013, (b) 2014, and (c) 2015 IOPs. The total number of rain gauges was 1,269 within the analysis area.

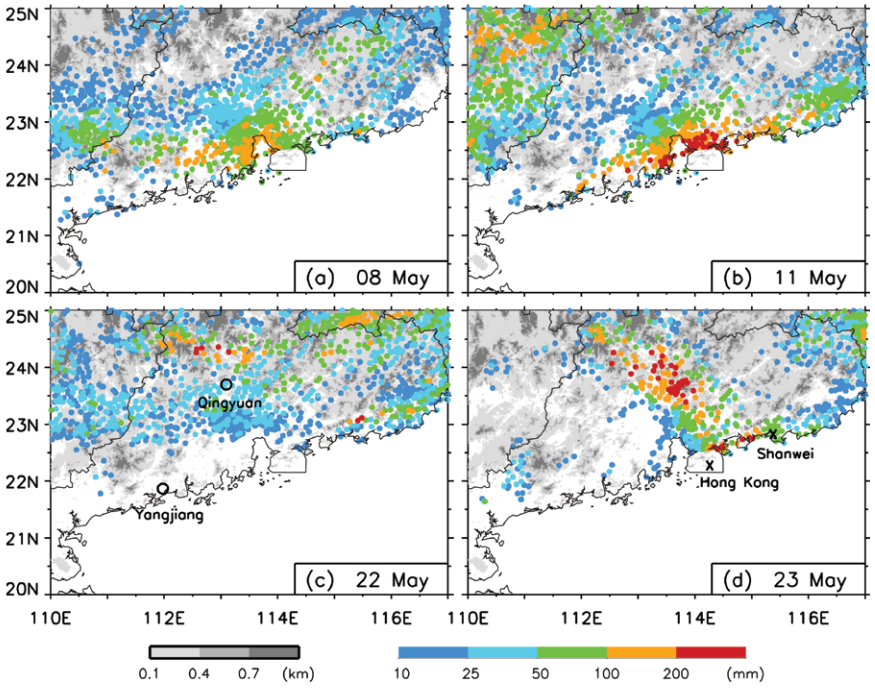

Fig. 4. Distribution of daily (0000–0000 BST) rainfall (mm) over the SCMREX enhanced observing area (orange rectangle in Fig. 2a) on (a) 8, (b) 11, (c) 22, and (d) 23 May 2014. Gray shading represents topography. The black circles in (c) denote the locations of the sounding stations at Qingyuan and Yangjiang, while the black crosses in (d) denote the locations of the operational S-band radars at Hong Kong and Shanwei.

(Fig. 4d). The extreme-rain-producing MCS consisted of numerous well-defined, southwest–northeast-oriented, band-shaped convective precipitation regions with reflectivity >35 dB*Z* (simply referred to herein as rainbands) during its life-span (Figs. 5g,h), exhibiting "band training" of the rainbands along the MCS (Luo et al. 2014). The rainbands, with a length of about 50 km, appeared quasi-stationary and moved little, continuously generating rain over the same areas for nearly 20 h (i.e., 0030–2030 BST). The rainband-training organization of extreme-rain-producing MCS has recently been noticed in east–central China during the mei-yu season (Luo et al. 2014), the western Guangdong coastal area on 10 May 2013 (Wang et al. 2014), and the eastern Guangdong coastal area on 20 May 2015 (Wu and Luo 2016).

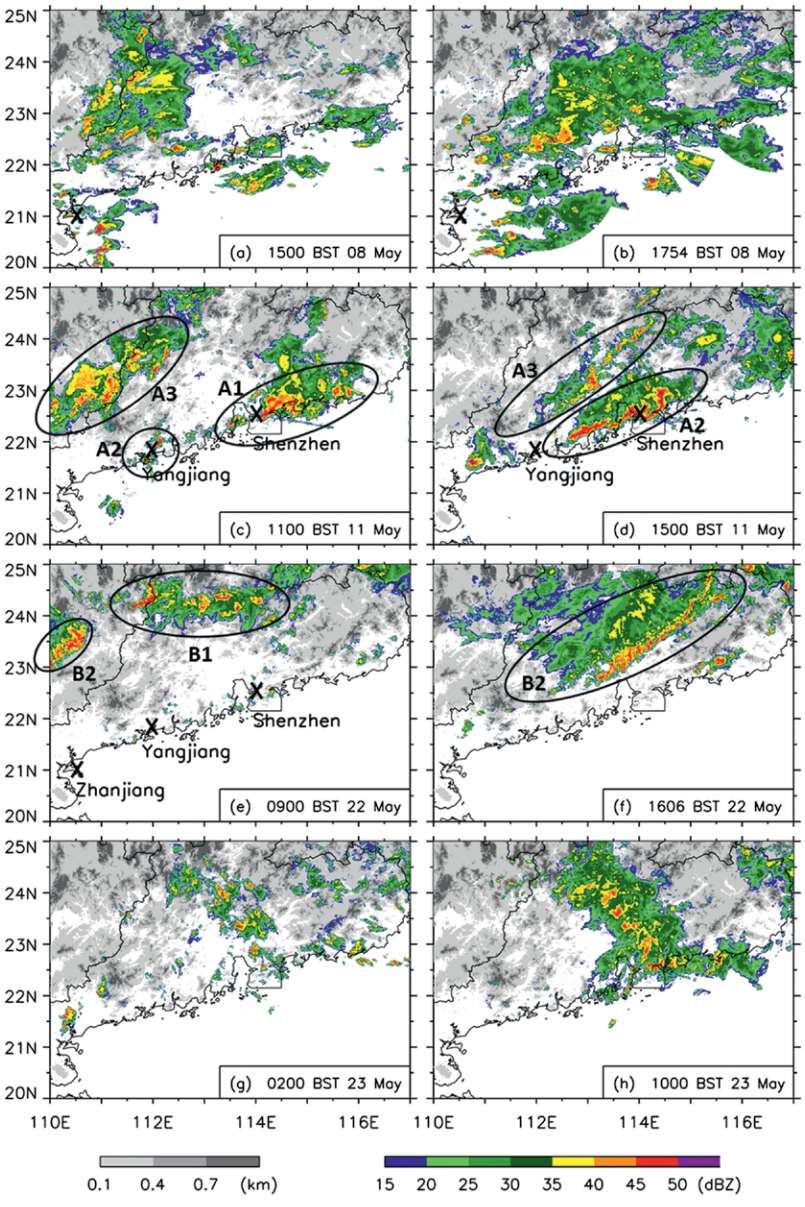

Fig. 5. Radar reflectivity at 3-km altitude MSL in the enhanced observing area (orange rectangle in Fig. 2a) derived from nine operational weather radars (eight in Guangdong and one in eastern Guangxi) at two selected times on (a),(b) 8, (c),(d) 11, (e),(f) 22, and (g),(h) 23 May 2014. Gray shading represents topography. The black crosses denote the locations of the operational S-band radars at Zhanjiang, Yangjiang, and Shenzhen. Ellipses in (c), (d), (e), and (f) denote the individual MCSs on 11 and 22 May, respectively.

Environmental conditions. Figure 6 shows synoptic background in which the heavy precipitation occurred over southern China on 8, 11, 22, and 23 May 2014. Of significance is that southern China was dominated by southwesterly flows with relatively high equivalent potential temperature θ_e air in the lower troposphere; that is, the heavy precipitation took place in the warm sector. There was a northeast–southwest-oriented shear line on 11 and 22 May (Figs. 6b,c) that was at least 200–300 km away from the heavy rainfall region of interest. Near the southwestern edge of the shear line was the linear-shaped MCS on 11 (A3 in Figs. 5c and 5d) and 22 May (B2 in Figs. 5e and 5f) initiated in Guangxi.

The environmental conditions of the precipitation systems on the rainy days were characterized by moderate (about 500–800 J kg^{-1} on 8 May) to large (about 2,400–3,000 J kg^{-1} on 22 May) convective available potential energy (CAPE), very small convective inhibition (CIN; mostly about 10 J kg^{-1} or less), and high moisture content (precipitable water of about 50–64 mm; e.g., Fig. 7). High correlations between low-level jets (LLJs) and heavy rainfall events have been noticed in the United States (Maddox et al. 1979; Schumacher and Johnson 2008) and northern Taiwan (Chen and Yu 1988). A signature of southwesterly LLJs was more evident on 11 and 22 May relative to 8 and 23 May 2014 (cf. Figs. 6b,c and Figs. 6a,d). Collective

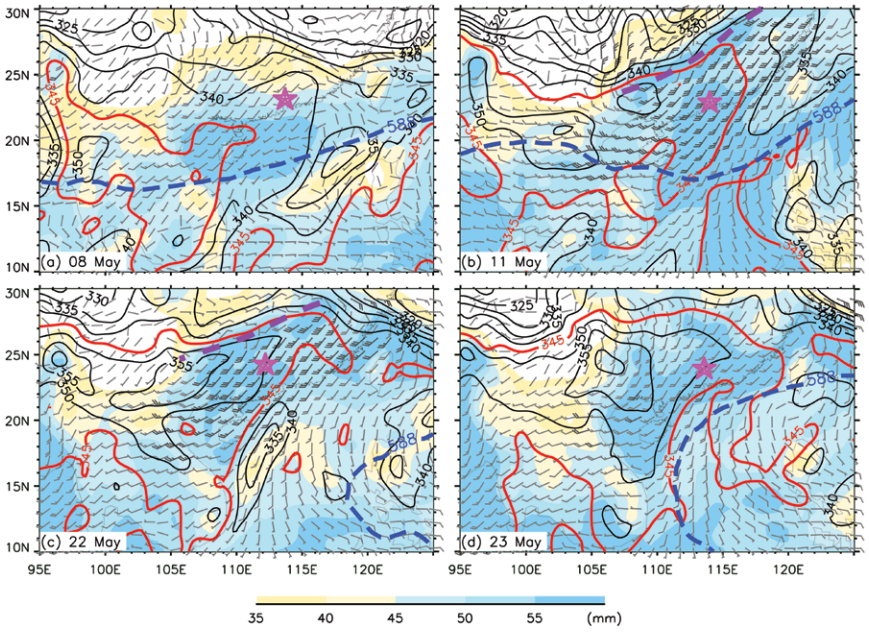

Fig. 6. The 850-hPa level from the European Centre for Medium-Range Weather Forecasts (ECMWF) interim reanalysis at 0800 BST on (a) 8, (b) 11, (c) 22, and (d) 23 May 2014, showing the equivalent potential temperature θ_e (black contours at intervals of 5 K, with the 345-K contour in red) superimposed with horizontal wind barbs and precipitable water (mm; shaded). A full barb is 5 m s^{-1}. Shear lines at 850 hPa are shown by thick dashed purple lines. The 588-dgpm contours of the geopotential height at 500 hPa are denoted by blue dashed lines. Pink markers denote locations of the heavy rainfall of interest on the corresponding days.

analysis of the data from the dense mesonets, wind profilers, and radars suggests that LLJ in the PBL, topography in northern Guangdong, and a cold pool left behind by previous-day convection appear to play an important role in the convective triggering and maintenance for the case on 23 May 2014. However, relationships between the conditions of low-level wind fields and the location of convective initiation that led to the formation of the heavy-rain-producing MCSs in southern China during the presummer rainy season deserve further investigation.

Polarimetric radar measurements. For the MCS over southwestern Guangdong in the late afternoon of 8 May 2014 (Figs. 8a, 5b) and the quasi-linear MCS over central Guangdong on the 22 May afternoon (Fig. 8b; B2 in Fig. 5f), range height indicator (RHI) scans were taken using the Heshan C-POL radar. The corresponding C-POL polarimetric measurements of the vertical cross sections (dashed lines in Fig. 8) are given in Fig. 9, showing the microphysical characteristics associated with the two MCSs. The RHI scan on 8 May went through a convective precipitation region (at about 43–55 km in Figs. 9a–d) embedded within wider stratiform precipitation areas. The convective precipitation within the MCS was characterized by the strong reflectivity ($Z_H \approx 50$–55 dBZ) associated with a column of high values of differential reflectivity ($Z_{DR} > 1.0$ dB) and specific differential phase shift ($K_{DP} > 4.0°$ km^{-1}) at about 45–48 km (see Figs. 9a–c, respectively). As Z_{DR} provides information about the oblateness of particles and K_{DP} depends on liquid water content (Bringi and Chandrasekar 2001), the positive Z_{DR} and K_{DP} column suggest raindrops extending up to 5.5-km altitude, about 0.9 km above the 0°C level (4.6 km according to sounding data). At 50–54 km in Figs. 9a–c, the values of Z_H, Z_{DR}, and K_{DP} increase from the 0°C level downward, suggesting a signature of warm rain. The stratiform precipitation regions were characterized by a brightband signature of low values of zero-lag cross-correlation coefficient (ρ_{HV} = 0.92–0.95) and high values of Z_H (about 35–40 dBZ) and Z_{DR} (about 1.0 dB) at 0°C level. On the other hand, the RHI scan on 22 May (Figs. 9e–h) mainly detected convective precipitation regions and the adjacent anvil clouds. The stronger and deeper convection on 22 May had large Z_H (about 50–55 dBZ) extending up to 7 km at about 33–35 km in Fig. 9e, well above the 0°C level (5.2 km according to sounding data). The lower ρ_{HV} (0.94–0.96) from the 0°C level to 7 km in the deep convective region (at about 33–35 km in Fig. 9h) suggests mixtures of ice (hail or irregular snow) and raindrops. In the meantime, the high values of K_{DP} (3.0°–3.5°C km^{-1}) and Z_{DR} (1.25–1.75 dB) in the lower-topped convection (at about 27–30 km in Fig. 9e) were located at 2–4-km altitudes. Below 2-km altitude, the K_{DP} and Z_{DR} decreasing toward the ground suggest breakup of large raindrop by the updraft.

PRELIMINARY RESEARCH HIGHLIGHTS.

Impact of assimilating WPR data on convection-permitting QPF. Vertical profiles of horizontal winds

measured by 14 WPRs over Guangdong were assimilated into a partial-cycle data assimilation system based on the three-dimensional variational method, using the Global/Regional Assimilation and Prediction System (GRAPES; Zhang and Shen 2008; Chen et al. 2008; Xue et al. 2008) with horizontal resolution of 0.03° × 0.03° in regular latitude–longitude coordinates. The impact of assimilating the WPR data on the 0–12-h QPF in southern China during May 2014 was evaluated by comparing the forecasts from two monthly continuous experiments: one with the WPR data assimilated (WPR_DA) and the other without it (no_WPR_DA). In each of the two experiments, analysis forecast cycles over a 30-day period in May 2014 were performed.

The comparison results indicate that assimilating the quality-controlled WPR data significantly improves the 0–6-h forecasts of the vertical structures of meteorological variables (e.g., *U* wind shown in Fig. 10a) and the diagnostic fields at the surface (e.g., the surface wind field in Fig. 10b). For example, the root-mean-square error (RMSE) of *U* wind at 200 hPa decreased from 5.71 to 5.31 m s^{-1}; the RMSE of the 10-m wind speed decreased from 3.48 to 3.13 m s^{-1} for the 3-h lead time. WPR_DA also improves the QPF skill throughout the 12-h

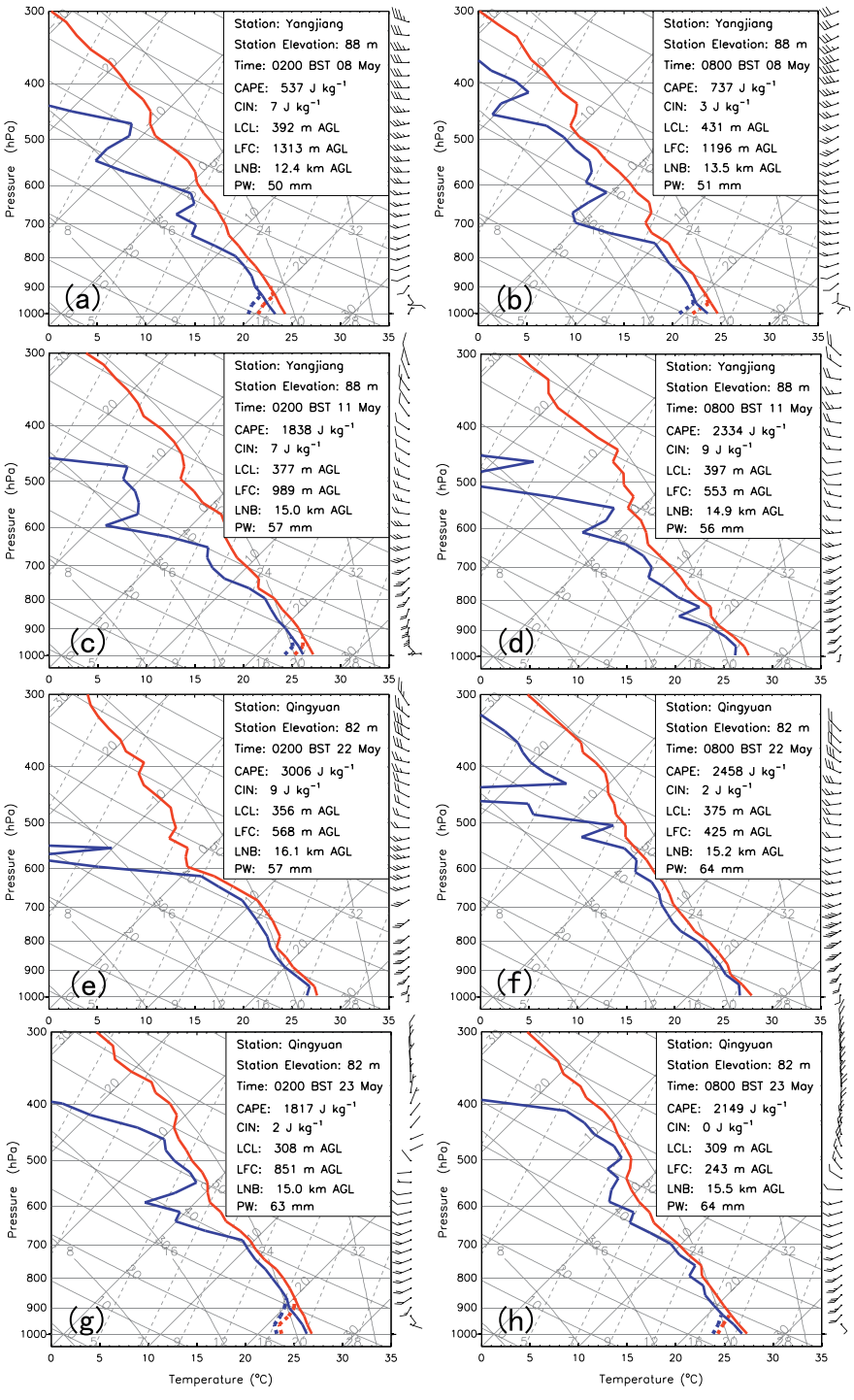

FIG. 7. Skew *T*-log*p* diagram at Yangjiang sounding station (59663) at (left) 0200 and (right) 0800 BST on (a),(b) 8 and (c),(d) 11 May 2014. As in (a)–(d), but for Qingyuan sounding station (59280) on (e),(f) 22 and (g),(h) 23 May 2014. The soundings on 8 May, at 0200 BST 11 May, and on 23 May were influenced by rain evaporative cooling near the surface and corrected based on the observations from the surface AWSs around the sounding station. The original soundings without the correction are shown in the panels as dashed lines, while the corrected soundings are shown as solid lines. The values of CAPE, CIN, lifting condensation level (LCL), level of free convection (LFC), and level of neutral buoyancy (LNB) were calculated for the mass-weighted near-surface air (0–500 m) after the correction.

forecast period by reducing the predicted spurious precipitation and alleviating overestimations and false alarms. The biases in the heavy rainfall (>20 mm h^{-1}) forecast were reduced by about 30% (Fig. 10c). Moreover, assimilating the WPR data improves the fractions skill score (FSS; Roberts 2008; Mittermaier and Roberts 2010) by 12% for the heavy rainfall (>20 mm h^{-1}) prediction at mesoscale (about 200 km; Fig. 10d) and by 31% for the extremely heavy rainfall (>40 mm h^{-1}) prediction at smaller scales (about 25 km; not shown). Further case studies suggest that the improved representations of wind and moisture at the lower levels after assimilating the WPR data lead to more reasonable descriptions of convective development and the associated rainfall production (Zhang et al. 2016).

Improving a cloud microphysical parameterization scheme. The squall line that occurred on 22 May 2014 was explicitly simulated in nonhydrostatic and convection-permitting configuration, with a two-way triply nested domain (grid spacing of 27, 9, and 3 km), using the Advanced Research version of the Weather Research and Forecasting (WRF-ARW; Skamarock et al. 2008) Model. Several microphysical schemes, including the State University of New York at Stony Brook bulk microphysical parameterization (SBU-YLIN) scheme (Lin and Colle 2011) and Morrison scheme (Morrison et al. 2005), were applied for comparing the simulations of the squall line. All the domains were initialized at 1200 UTC (or 2000 BST) 21 May 2014 and integrated for 24 h. The National Centers for Environmental Prediction (NCEP) Final Operational Global Analysis (FNL) with a 6-h interval was used for the model initial and outermost lateral boundary conditions.

Surface cooling rates, an indication of the cold pool strength, were as strong as −3 K in the observations at 0800 UTC (Fig. 11d). However, they are nearly zero in the simulation with the original SBU-YLIN scheme (Fig. 11a). This disagreement largely explains why

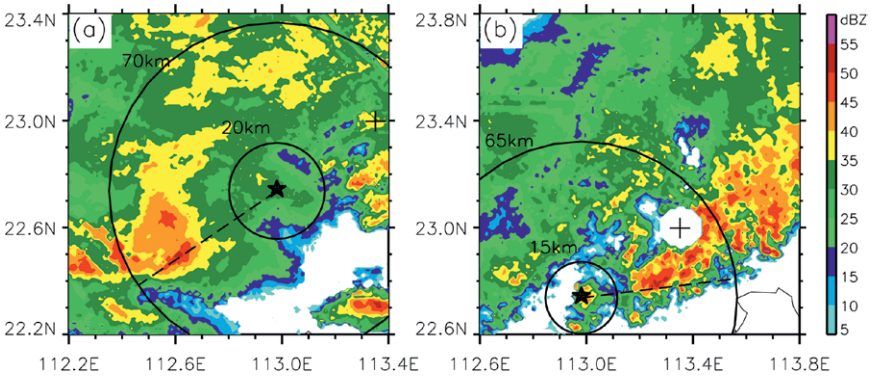

Fig. 8. CAPPI at 3 km MSL derived from the Guangzhou S-band radar volumetric scans at about (a) 1754 BST 8 May and (b) 1606 BST 22 May 2014. The cross and star denote locations of the Guangzhou radar and the Heshan C-POL radar, respectively. Black dashed lines represent the locations of the vertical cross sections shown in Fig. 9.

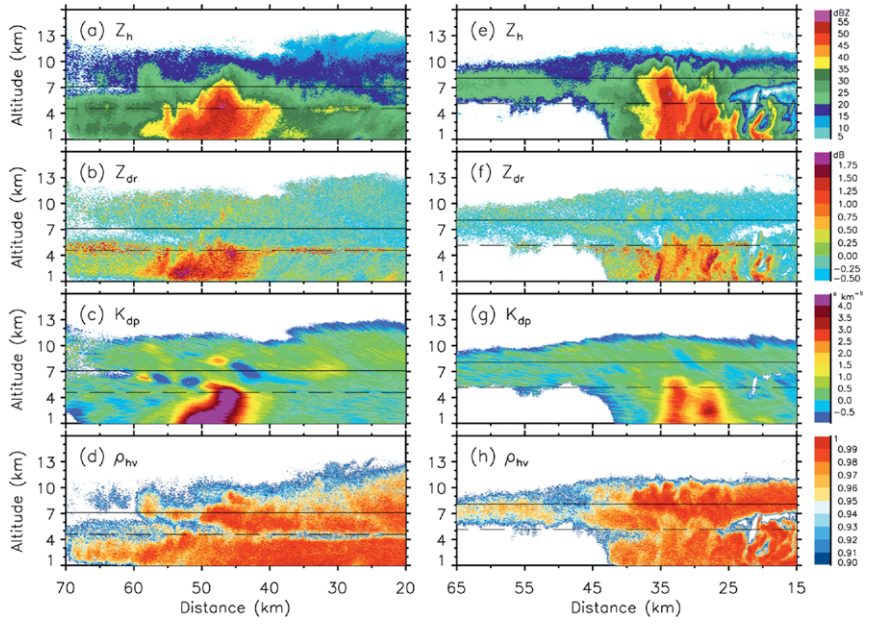

Fig. 9. Vertical cross section at about 1752 BST 8 May of the Heshan C-POL measurements of (a) reflectivity Z_H, (b) differential reflectivity Z_{DR}, (c) specific differential phase K_{DP}, and (d) correlation coefficient ρ_{HV}. The black dashed and solid lines represent the 0°C level (4.6 km) and −15°C level (7 km), respectively, according to sounding data. (e)–(h) As in (a)–(d), respectively, but at about 1604 BST 22 May 2014; the 0° and −15°C levels are 5.2 and 8.1 km, respectively.

the squall line was missed in this simulation as the presence of a cold pool is critical for the maintenance and movement of a squall line (Rotunno et al. 1988). Through a series of sensitivity tests and detailed investigations, the failure of the original SBU-YLIN scheme to capture the evolution of the squall line is traced down to two major factors: turnoff of rain evaporation in environment with relative humidity greater than 90%, and the saturation adjustment method of Tao et al. (1989). Rain evaporation tendency in the scheme is computed based on the conditions at the beginning of each time step but applied over the whole length of the time step. This might lead to supersaturation during this time step due to evaporative cooling, which makes rain evaporation nonphysical, especially for large time steps. In the original SBU-YLIN scheme the solution for partially preventing this was to disallow rain evaporation to increase relative humidity (RH) above 90% within the grid cell at the end of the time step based on the initial saturation mixing ratio. As a result, rain evaporation is inhibited below the cloud base since RH is greater than 90% most of the time during the simulation. This is undesirable and we adopted a new method proposed by P. N. Blossey (2016, personal communication) in which the amount of rain evaporation that would produce saturation (accounting for the change in saturation mixing ratio due to evaporative cooling) is calculated and the evaporation is kept smaller than 0.9 of this amount in magnitude. The modification enables the rain evaporation even in a relatively moist environment, which favors the initiation of the cold pool and the maintenance of the squall line. In the saturation adjustment method of Tao et al. (1989), saturation vapor pressure was calculated by the gridbox temperature without considering the cooling associated with cloud evaporation and ice sublimation, that is, only suitable for cloud-free situation. This can lead to frequent fluctuations between cloud-free and cloudy situations in a grid box. To alleviate this problem, the calculation of saturation vapor pressure was refined by including the cooling effect associated with cloud evaporation and ice sublimation and thus became more suitable for both cloud-free and cloudy situations. This fix further improved the simulation of the squall line, including its movement and morphology.

With these two modifications, the simulation is significantly improved in the strength of the cold pool, movement of the squall line, the total precipitation produced, and the trailing stratiform precipitation (Fig. 11b). These results suggest that the weakness of

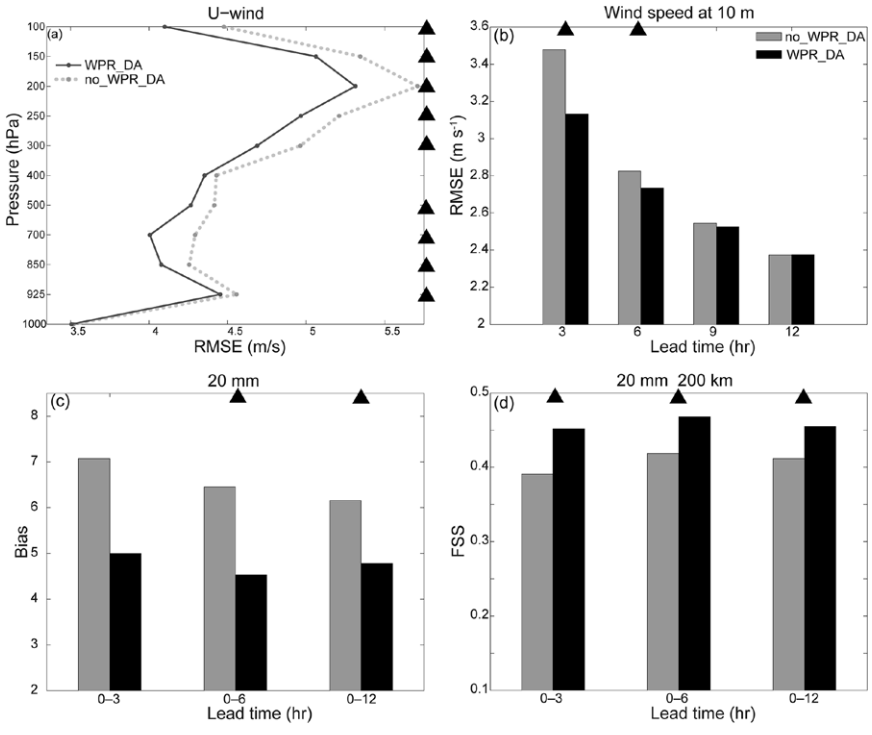

Fig. 10. (a) Vertical profiles of RMSEs of the 12-h forecasts of *U* wind with respect to radiosonde observations in the two monthly continuous experiments with (WPR_DA; solid lines) and without (no_WPR_DA; dotted lines), the WPR measurements being assimilated. (b) RMSEs for the forecasts of horizontal wind speed at 10-m altitude AGL with respect to surface observations in no_WPR_DA (light bars) and WPR_DA (dark bars) as a function of lead time. (c) Bias for the forecasts of 1-h accumulated precipitation (>20 mm) averaged over different lead times in no_WPR_DA (light bars) and WPR_DA (dark bars). (d) FSS for the forecasts of 1-h accumulated precipitation averaged over different lead times with a precipitation threshold of 20 mm and a neighborhood length of 200 km in no_WPR_DA (light bars) and WPR_DA (dark bars). Dark triangles indicate that the significance level of the difference of RMSE in (a) and (b), bias in (c), and FSS in (d) between WPR_DA and no_WPR_DA is greater than 90%.

the original SBU-YLIN scheme in simulating squall lines is not solely due to the small terminal velocity of precipitating ice as recently pointed out by Morrison et al. (2015). This example also highlights the importance of SCMREX for providing cases for model physics evaluation and improvement. More detailed analyses about the sensitivity to various cloud microphysical parameterization schemes, modifications to the original SBU-YLIN scheme, and the resultant impacts on the simulations as well as comparisons between a double-moment version of the SBU-YLIN scheme and its original single-moment version will be published in the future.

SUMMARY AND FUTURE RESEARCH. An extensive array of meteorological instrumentation was deployed during the SCMREX pilot field campaigns of 2013–15 to investigate the characteristics of mesoscale weather systems producing extreme rainfall over southern China during the presummer rainy season. Extreme daily rainfall was produced by long-lived MCSs with a linear alignment of convective cells that favored persistent and large rainfall accumulation over the same region. The characteristics of the extreme-rain-producing MCSs during SCMREX that led to heavy rainfall (their duration, organizational patterns, and quasi-stationary behavior) appear to be attributable to the characteristic environmental conditions during the presummer rainy season. Namely, these systems occurred in prevailing southwesterly monsoonal flows providing sufficient moisture even without the presence of an LLJ over complex underlying surfaces in southern China (e.g., land–sea contrast and mountains near the coasts and inland facilitating continuous convective initiation) and within a series of feedbacks from MCSs (i.e., convectively generated cold outflow boundaries where continuous convective initiation usually takes place), as discussed by Wang et al. (2014) and Wu and Luo (2016).

Further in-depth observational and modeling studies are necessary to achieve the scientific objectives of SCMREX. In particular, our ability to predict the timing and location of convective initiation is very limited, due partly to the lack of sufficient high-resolution observations and partly to the insufficient understanding of the impact of terrain, land surface

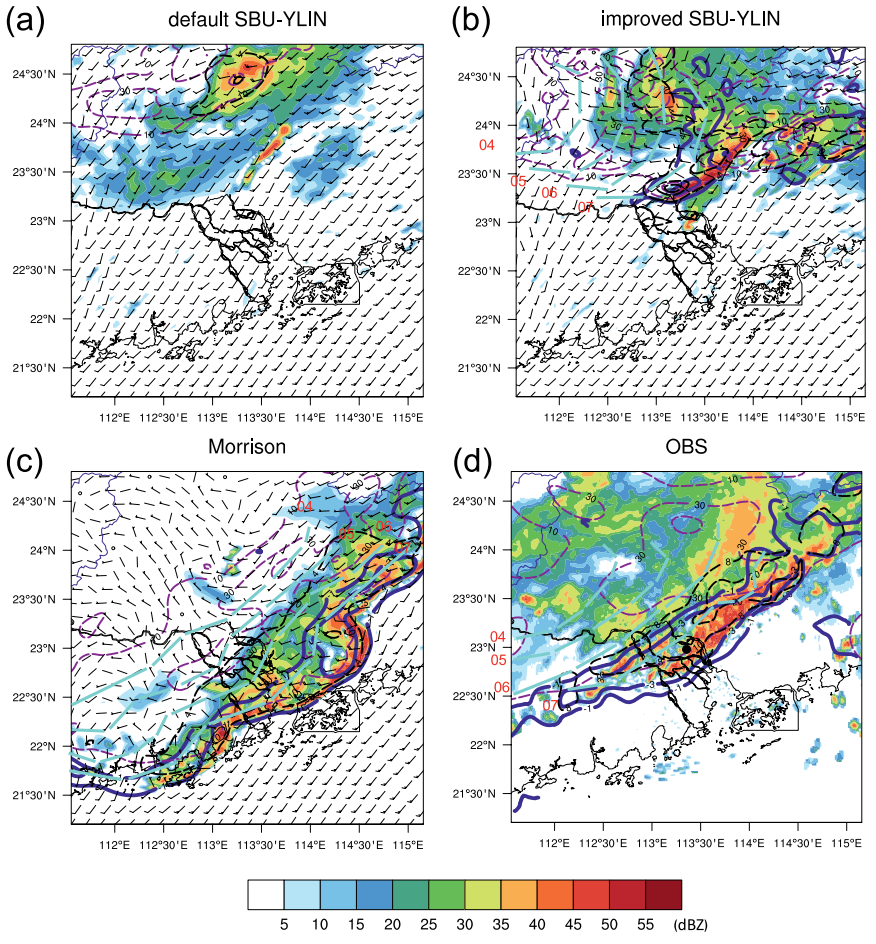

FIG. 11. Radar reflectivity (dBZ; color shaded) and wind barbs at 0.5 km MSL at 0800 UTC 22 May 2014, the 0400–0800 UTC total precipitation (mm; magenta dashed lines), surface air temperature changes from 0700 to 0800 UTC (K h^{-1}; blue solid lines), hourly precipitation ending at 0800 UTC (mm; black dashed lines), and the location of the squall line during the previous 4 h (cyan dashed lines with red number denoting the time) from simulations using (a) the default SBU-YLIN scheme, (b) the improved SBU-YLIN scheme, (c) the Morrison scheme, and (d) from the observations [no wind barbs in (d)]. The area covered by the −3 K h^{-1} contour of surface cooling rate is approximately an indication of the cold pool. The black dot in (d) depicts the location of the Guangzhou radar.

inhomogeneity, and convectively generated surface boundaries. For example, convective initiation appeared to be more favorable over the western Guangdong coast on 10 May 2013 (Wang et al. 2014) and western to central Guangdong coast 11 May 2014 (Figs. 5c,d), over the northern mountainous regions of Guangdong on 22 May 2014 (Fig. 5e), and over both northern Guangdong and eastern Guangdong coast on 23 May 2014 (Figs. 5g,h). Organizational modes and movement characteristics of MCSs also varied among the days and even on the same days (Fig. 5). More comprehensive studies are needed to reveal the underlying physical mechanisms to account for such differences. Moreover, measurements from the polarimetric radars, MRRs, MMCR, C-FMCW radar, and disdrometers will be analyzed more carefully in order to quantitatively unravel the characteristics of cloud and precipitation processes over southern China during the presummer rainy season and compare with those over other regions, for example, southern Taiwan during the Southwest Monsoon Experiment/Terrain-Influenced Monsoon Rainfall Experiment (SoWMEX/TiMREX; Jou et al. 2011). Results of numerical experiments using convection-permitting NWP models will be postprocessed using simulators such as the polarimetric radar data simulator (Jung et al. 2008) to make "apple to apple" comparisons with the observations. Such comparisons will facilitate further research development to improve the parameterizations of cloud–precipitation microphysics such as the SBU-YLIN scheme and a newly developed scheme based on observations over eastern China (Yin 2013). Furthermore, the impact study of assimilating WPR data on QPF (Zhang et al. 2016) will be extended to the operational weather radars and the polarimetric radars. Effects of land surface processes in the variability of ensemble simulations will also need to be investigated, such as by using different combinations of subprocesses and parameters in Noah-MP land surface model (LSM) of WRF (Niu et al. 2011).

ACKNOWLEDGMENTS. This work was jointly funded by the Public Welfare Scientific Research Projects in Meteorology (GYHY201406013, GYHY201406003, GYHY201306004, and GYHY201406007), Scientific Research Projects of the Chinese Academy of Meteorological Sciences (CAMS; 2014Z004), Outreach Projects of the State Key Laboratory of Severe Weather (2014LASW-B04 and 2014LASW-B05), and the National Basic Research Program of China (973 Program; 2012CB417202 and 2014CB441402). We would like to acknowledge the Hong Kong Observatory for their additional sounding observations and the data collection flight; the Guangdong Meteorological Bureau for providing the WPR data, the additional sounding observations, and logistical support; and the Center of Data Analysis and Application of CAMS for archiving SCMREX data. We would also like to thank the Guangxi Meteorological Bureau and the Hainan Meteorological Bureau for their additional sounding observations. This research is a Research and Development Project of the World Weather Research Programme (WWRP). The research plan is developed by the Monsoon Panel Expert Team on Severe Monsoon Weather of the WWRP Working Group on Tropical Meteorology Research.

REFERENCES

Bringi, V. N., and V. Chandrasekar, 2001: *Polarimetric Doppler Weather Radar-Principles and Applications.* Cambridge University Press, 636 pp.

Chen, D. H., and Coauthors, 2008: New generation of multiscale NWP system (GRAPES): General scientific design. *Chin. Sci. Bull.*, **53**, 3433–3445, doi:10.1007/s11434-008-0494-z.

Chen, G. T.-J., and C.-C. Yu, 1988: Study of low-level jet and extremely heavy rainfall over northern Taiwan in the mei-yu season. *Mon. Wea. Rev.*, **116**, 884–891, doi:10.1175/1520-0493(1988)116<0884:SOLLJA>2.0.CO;2.

Cummins, K. L., M. J. Murphy, E. A. Bardo, W. L. Hiscox, R. B. Pyle, and A. E. Pifer, 1998: A combined TOA/MDF technology upgrade of the U.S. National Lightning Detection Network. *J. Geophys. Res.*, **103**, 9035–9044, doi:10.1029/98JD00153.

Ding, Y. H., 1994: *Monsoons over China.* Kluwer Academic Publishers, 419 pp.

Doswell, C. A., III, H. E. Brooks, and R. A. Maddox, 1996: Flashflood forecasting: An ingredients-based methodology. *Wea. Forecasting*, **11**, 560–581, doi:10.1175/1520-0434(1996)011<0560:FFFAIB>2.0.CO;2.

Huang, S. S., 1986: *Heavy rainfall over Southern China in the Pre-Summer Rainy Season* (in Chinese). Guangdong Science and Technology Press, 244 pp.

Jou, B. J.-D., W.-C. Lee, and R. H. Johnson, 2011: An overview of SoWMEX/TiMREX and its operation. *The Global Monsoon System: Research and Forecast*, 2nd ed. C.-P. Chang, Ed., World Scientific, 303–318.

Jung, Y., G. Zhang, and M. Xue, 2008: Assimilation of simulated polarimetric radar data for a convective storm using the ensemble Kalman filter. Part I: Observation operators for reflectivity and polarimetric variables. *Mon. Wea. Rev.*, **136**, 2228–2245, doi:10.1175/2007MWR2083.1.

Lin, Y., and B. A. Colle, 2011: A new bulk microphysical scheme that includes riming intensity and temperature-dependent ice characteristics. *Mon. Wea. Rev.*, **139**, 1013–1035, doi:10.1175/2010MWR3293.1.

Liu, L., J. Zheng, Z. Ruan, Z. Cui, Z. Hu, S. Wu, G. Dai, and Y. Wu, 2015: Comprehensive radar observations of clouds and precipitation over the Tibetan Plateau and preliminary analysis of cloud properties. *J. Meteor. Res.*, **29**, 546–561, doi:10.1007/s13351-015-4208-6.

Luo, Y., 2017: Advances in understanding the early-summer heavy rainfall over south China. *The Global Monsoon System: Research and Forecast*, 3rd ed. C. P. Chang et al., Eds., World Scientific Series on Asia-Pacific Weather and Climate, Vol. 9, World Scientific, 215–226.

——, H. Wang, R. Zhang, W. Qian, and Z. Luo, 2013: Comparison of rainfall characteristics and convective properties of monsoon precipitation systems over south China and the Yangtze and Huai River basin. *J. Climate*, **26**, 110–132, doi:10.1175/JCLI-D-12-00100.1.

——, Y. Gong, and D.-L. Zhang, 2014: Initiation and organizational modes of an extreme-rain-producing mesoscale convective system along a mei-yu front in east China. *Mon. Wea. Rev.*, **142**, 203–221, doi:10.1175/MWR-D-13-00111.1.

Maddox, R. A., C. F. Chappell, and L. R. Hoxit, 1979: Synoptic and meso-α scale aspects of flash flood events. *Bull. Amer. Meteor. Soc.*, **60**, 115–123, doi:10.1175/1520-0477-60.2.115.

Mittermaier, M., and N. Roberts, 2010: Intercomparison of spatial forecast verification methods: Identifying skillful spatial scales using the fractions skill score. *Wea. Forecasting*, **25**, 343–354, doi:10.1175/2009WAF2222260.1.

Morrison, H., J. A. Curry, and V. I. Khvorostyanov, 2005: A new double-moment microphysics parameterization for application in cloud and climate models. Part I: Description. *J. Atmos. Sci.*, **62**, 1665–1677, doi:10.1175/JAS3446.1.

——, J. A. Milbrandt, G. H. Bryan, K. Ikeda, S. A. Tessendorf, and G. Thompson, 2015: Parameterization of cloud microphysics based on the prediction of bulk ice particle properties. Part II: Case study comparisons with observations and other schemes. *J. Atmos. Sci.*, **72**, 312–339, doi:10.1175/JAS-D-14-0066.1.

Niu, G.-Y., and Coauthors, 2011: The community Noah land surface model with multiparameterization options (Noah-MP): 1. Model description and evaluation with local-scale measurements. *J. Geophys. Res.*, **116**, D12109, doi:10.1029/2010JD015139.

Roberts, N. M., 2008: Assessing the spatial and temporal variation in the skill of precipitation forecasts from an NWP model. *Meteor. Appl.*, **15**, 163–169, doi:10.1002/met.57.

Rotunno, R., J. B. Klemp, and M. L. Weisman, 1988: A theory for strong, long-lived squall lines. *J. Atmos. Sci.*, **45**, 463–485, doi:10.1175/1520-0469(1988)045<0463:ATFSLL>2.0.CO;2.

Schönhuber, M., G. Lammer, and W. Randeu, 2007: One decade of imaging precipitation measurement by 2D-video-distrometer. *Adv. Geosci.*, **10**, 85–90, doi:10.5194/adgeo-10-85-2007.

Schumacher, R. S., and R. H. Johnson, 2008: Mesoscale processes contributing to extreme rainfall in a midlatitude warm-season flash flood. *Mon. Wea. Rev.*, **136**, 3964–3986, doi:10.1175/2008MWR2471.1.

Skamarock, W. C., and Coauthors, 2008: A description of the Advanced Research WRF version 3. NCAR Tech. Note NCAR/TN-475+STR, 113 pp., doi:10.5065/D68S4MVH.

Tao, W.-K., J. Simpson, and M. McCumber, 1989: An ice-water saturation adjustment. *Mon. Wea. Rev.*, **117**, 231–235, doi:10.1175/1520-0493(1989)117<0231:AIWSA>2.0.CO;2.

Wang, H., Y. Luo, and B. Jou, 2014: Initiation, maintenance, and properties of convection in an extreme rainfall event during SCMREX: Observational analysis. *J. Geophys. Res. Atmos.*, **119**, 13 206–13 232, doi:10.1002/2014JD022339.

Wu, M., and Y. Luo, 2016: Mesoscale observational analysis of lifting mechanism of a warm-sector convective system producing the maximal daily precipitation in China mainland during pre-summer rainy season of 2015. *J. Meteor. Res.*, **30**, 719–736, doi:10.1007/s13351-016-6089-8.

Xia, R., D.-L. Zhang, and B. Wang, 2015: A 6-yr cloud-to-ground lightning climatology and its relationship to rainfall over central and eastern china. *J. Appl. Meteor. Climatol.*, **54**, 2443–2460, doi:10.1175/JAMC-D-15-0029.1.

Xue, J. S., S. Y. Zhuang, G. F. Zhu, H. Zhang, Z. Liu, Y. Liu, and Z. Zhuang, 2008: Scientific design and preliminary results of three-dimensional variational data assimilation system of GRAPES. *Chin. Sci. Bull.*, **53**, 3446–3457, doi:10.1007/s11434-008-0416-0.

Yin, J., 2013: The study on observation and parameterization of cloud-precipitation microphysical properties over East Asia (in Chinese). Ph.D. thesis, Zhejiang University, 163 pp.

Zhang, R. H., and X. S. Shen, 2008: On the development of the GRAPES—A new generation of the national operational NWP system in China. *Chin. Sci. Bull.*, **53**, 3429–3432, doi:10.1007/s11434-008-0462-7.

——, Y. Q. Ni, L. P. Liu, Y. Luo, and Y. Wang, 2011: South China Heavy Rainfall Experiments (SCHeREX).

J. Meteor. Soc. Japan, **89A**, 153–166, doi:10.2151/jmsj.2011-A10.

Zhang, X. B., Y. Luo, Q. Wan, W. Ding, and J. Sun, 2016: Impact of assimilating wind profiling radar observations on convection-permitting quantitative precipitation forecasts during SCMREX. *Wea. Forecasting*, **31**, 1271–1292, doi:10.1175/WAF-D-15-0156.1.

Zhang, Y. J., W. T. Lu, Y. Zhang, D. Zheng, L. Chen, S. Chen, and X. Yan, 2014: Evaluation for the performance of the Guangdong-Hongkong-Macau lightning location system. *Proc. 23th Int. Lightning Detection Conf.*, Tucson, Arizona, Vaisala, 1–5. [Available online at www.vaisala.com/en/events/ildcilmc/archive/Pages/ILDC-2014-archive.aspx.]

Zhou, X.-J., 2003: *Heavy Rainfall Experiment in South China during Pre-summer Rainy Season (HUAMEX), 1998* (in Chinese). China Meteorological Press, 220 pp.

Zhu, X., and J. Zhu, 2004: New generation weather radar network in China (in Chinese). *Mater. Sci. Technol.*, **32**, 255–258.

Radar and Atmospheric Science: A Collection of Essays in Honor of David Atlas

Edited by Roger M. Wakimoto and Ramesh Srivastava

This monograph pays tribute to one of the leading scientists in meteorology, Dr. David Atlas. In addition to profiling the life and work of the acknowledged "Father of Radar Meteorology," this collection highlights many of the unique contributions he made to the understanding of the forcing and organization of convective systems, observation and modeling of atmospheric turbulence and waves, and cloud microphysical properties, among many other topics. It is hoped that this text will inspire the next generation of radar meteorologists, provide an excellent resource for scientists and educators, and serve as a historical record of the gathering of scholarly contributions honoring one of the most important meteorologists of our time.

Radar and Atmospheric Science: A Collection of Essays in Honor of David Atlas

Aug 2003. Meteorological Monograph Series, Vol. 30, No. 52; 270 pp, hardbound; ISBN 1-878220-57-8; AMS code MM52.

Price $75.00 list/$55.00 member

To place an order point your Web browser to www.ametsoc.org/amsbookstore

AMS BOOKS

RESEARCH ◆ APPLICATIONS ◆ HISTORY